



Published in final edited form as:

Commun Nonlinear Sci Numer Simul. 2018 March ; 56: 330–343. doi:10.1016/j.cnsns.2017.08.020.

Predicting seizure by modeling synaptic plasticity based on EEG signals - a case study of inherited epilepsy

Honghui Zhang^a, Jianzhong Su^{b,*}, Qingyun Wang^c, Yueming Liu^b, Levi Good^d, and Juan Pascual^d

^aSchool of Natural and Applied Science, Northwestern Polytechnical University, Xi'an, Shaanxi, 710072, China

^bDepartment of Mathematics, The University of Texas at Arlington, Texas, 76019, USA

^cDepartment of Dynamics and Control, Beihang University, Beijing, 100191, China

^dDepartment of Neurology, University of Texas Southwestern medical center at Dallas, Dallas, Texas, 75390, USA

Abstract

This paper explores the internal dynamical mechanisms of epileptic seizures through quantitative modeling based on full brain electroencephalogram (EEG) signals. Our goal is to provide seizure prediction and facilitate treatment for epileptic patients. Motivated by an earlier mathematical model with incorporated synaptic plasticity, we studied the nonlinear dynamics of inherited seizures through a differential equation model. First, driven by a set of clinical inherited electroencephalogram data recorded from a patient with diagnosed Glucose Transporter Deficiency, we developed a dynamic seizure model on a system of ordinary differential equations. The model was reduced in complexity after considering and removing redundancy of each EEG channel. Then we verified that the proposed model produces qualitatively relevant behavior which matches the basic experimental observations of inherited seizure, including synchronization index and frequency. Meanwhile, the rationality of the connectivity structure hypothesis in the modeling process was verified. Further, through varying the threshold condition and excitation strength of synaptic plasticity, we elucidated the effect of synaptic plasticity to our seizure model. Results suggest that synaptic plasticity has great effect on the duration of seizure activities, which support the plausibility of therapeutic interventions for seizure control.

Keywords

inherited seizures; seizure prediction; EEG; synaptic plasticity

1. Introduction

EEG is considered as the gold standard for inherited seizure detection among other seizure detection modalities [1, 2, 3], since it is non-invasive and can repeatedly record the brain

* su@uta.edu; Tel: 817-272-3261.

activities of patients for a long duration for analyzing patients' conditions and monitoring treatments [4, 5, 6], including evaluating the most suitable anti-epileptic medicine, determining the seizure focus, finding out the causes for impaired cognitive function. Clinical diagnosis and treatment of patients have driven recent research on epileptic seizure prediction based on EEG data [7], including both physiological experiments [8, 9, 10, 11] and model analysis [12, 13, 14].

Epileptic seizure prediction remains a challenging problem. Considerable efforts have been made to predict seizures focused on several types of features that discriminate between interictal and preictal states [15]. A number of statistical features of seizures and non-seizures can be extracted based on continuously recorded EEG data which can improve prediction accuracy. These include univariate features, such as the power spectral density or autoregressive modeling coefficients of single EEG channels, as well as bivariate features that measure pairwise correlations between EEG channels, such as maximum cross correlation or phase synchrony [16, 17]. Signal analysis techniques may transform ictal EEG signals in a way that inherent hidden structures are revealed. Due to the nonstationary and nonlinear nature of EEG signals, time domain analysis, frequency domain analysis, time-frequency domain analysis, wavelet transform analysis and other nonlinear methods have been used to distinguish EEG signals in normal period and during seizures [18, 19, 20]. These models usually reflect statistical features of seizures.

Alternatively, dynamical seizure model established by electrical phenomenon can also contribute to seizure prediction. Through dynamics modeling analysis, we can obtain insight about the mechanics and symptoms of disease, and then to improve the prediction. Deriving a simple and functional dynamic model that represents the onset of epileptic seizures is attractive [21, 22, 23]. Taylor et al. demonstrated epileptic spike-wave discharges in an extended version of Amari's neural field model, and used a computational model of epilepsy spike-wave dynamics to evaluate the effectiveness of a pseudospectral method to simulate absence seizures [24, 25]. The model leads to a prototypic equation of clinical epileptic dynamics in time and space. By using a biophysically based model, Chen et al. pointed out that the typical absence seizure activities can be controlled and modulated by direct GABAergic projections from substantia nigra pars reticulata (SNr) to either either the thalamic reticular nucleus (TRN) or the specific relay nuclei (SRN) of thalamus [26]. A number of studies have shown that synaptic plasticity contributes to the pathophysiology of epilepsy and other neurological and psychiatric disorders [27, 28]. Alamir et. al proposed a dynamical seizure model which demonstrated that epileptic activity is induced by a high level of synchrony that is due to a disturbed balance between two opposing mechanisms: A basic functional desynchronization mechanism and a synaptic based synchronization mechanism [29].

The mapping of human brain function in real time has suffered from a lack of innovation in the past decade. Even though brain-imaging tools, e.g. functional magnetic resonance imaging (fMRI), positron emission computed tomography (PET), magnetic encephalography (MEG) are widely used, they are limited by low spatial and temporal resolution, cost, mobility and suitability for long-term monitoring. For example, fMRI has the advantage of providing spatially-resolved data, but suffers from an ill-posed temporal

inverse problem, i.e., a map with regional activations does not contain information about when and in which order these activations have occurred [30]. In contrast, EEG signals have been successfully used to obtain useful diagnostic information in clinical contexts. Further, they present the advantage to be highly portable, inexpensive, and can be acquired at the bedside or in real-life environments with a high temporal resolution. EEG offers the possibility of measuring the electrical activity of neuronal cell assemblies on the sub millisecond time scale [31, 32, 33].

While there is successful seizure research in animal model and seizure patients, seizure modeling based on the dynamic features of EEG information is not common. Motivated by previous work [29], we will investigate the dynamics of inherited seizure based on clinical EEG of one patient recordings as a case study. We will follow later with additional data to further modify and validate the modeling strategy. We will describe the methodology in section 2, including clinical neonatal EEG signals, dynamical seizure model and synchronization measurement. Then in section 3, simulation results will be provided under different situations to validate our model. Then, section 4 compares the effects of synaptic plasticity on the dynamics of the seizure network. Conclusions and discussion are in section 5.

2. Methods

EEG records a weighted average of local field potential at various brain areas by a group of electrodes placed on the scalp. EEG data can be used to diagnose neural diseases, such as epilepsy, schizophrenia, manic depression and mental disorders. Particularly, neonatal seizures result from synchronous discharges from groups of neurons and manifest as periods of heightened periodicity in the EEG lasting for more than 10s [34]. Thus EEG has been used as a detection modality for seizure patients.

2.1. Patient data from EEG recording

The sample data is recorded from a patient (age, gender) who was diagnosed with Glucose Transporter Type I Deficiency (G1D). G1D is a rare genetic defect that affects infants under the age of 3 years. When properly diagnosed, dietary treatment with high fat content can relieve symptoms. The EEG imaging of G1D patients provides helpful insight of the dynamic mechanism of seizure formation in G1D patients. As established in Pascual and Ronen [35] and Pascual [36], G1D patients had a well-defined epileptic episodes. In a recording of 2000 seconds, 103 nearly identical seizure episodes are captured. In this paper, the EEG data is from one patient as mentioned above.

2.2. Neonatal seizure EEG data

The EEG data acquired for our study is through a standard 32-channel EEG recordings (brain Tree), and the duration of each data acquisition is about 1010s. One channel is used as ground, and 31 channels are used for analysis. Figure 1(a), 1(b) depict two seizure periods of EEG data from the four channels(Fp1, Fp2, F3, F4), in which the high amplitude period representing denotes the seizure onset lasts 5s–10s, and the interest seizure time represented by the lower amplitude is also in this range.

It is known that there are usually artifacts in the EEG data recordings, including power-line interference, motion artifact, noise and other environmental factors. The data was processed through pre-processing with removal of artifacts and de-noise. Desired numerical analysis should be conducted after data becomes cleaned up. Figure 2(a), 2(b) present the de-noised EEG data of 31 channels which still display some harshness, sharpness and fluctuation. Then for further data smoothing, we use a second order of Fourier function fitting. EEG signals become clearer, and the effect after treatment can be observed in Figure 2(c),2(d). After the Fourier curve fitting, needed feature such as peaks and valleys persisted, and also the correlation structure of multi-channels EEG recordings will be preserved, which is a focus of our study.

The correlation matrix of all possible pairs of EEG channels of has been proposed to quantify the degree of underlying neuronal connectivity [37]. We follow the Pearson product-moment correlation coefficient in the term:

$$r = \frac{\sum_{i=1}^N (X_i - \bar{X})(Y_i - \bar{Y})}{\sqrt{\sum_{i=1}^N (X_i - \bar{X})^2} \sqrt{\sum_{i=1}^N (Y_i - \bar{Y})^2}}, \quad (1)$$

where X_i, Y_i are EEG time sequences at two different electrode channels X and Y . In generally, when $|r|$ is greater than 0.8, it is considered that there is a strong linear correlation between the two channels. Therefore, in our simulations, if the correlation coefficient of two EEG signals is greater than 0.8, then they will be considered as strongly coupled with each other and will be in one group. For example, the connection relationship of EEG data for period of 400s–440s is shown in Figure 3. All 31 channels can be divided into four coupled groups or clusters: ① $A_1 = [1, 5, 7, 9, 11, 13, 15, 21, 25, 27, 29, 31]$; ② $A_2 = [2, 3, 4, 7]$; ③ $A_3 = [6, 12, 14, 16, 26, 28, 30]$; ④ $A_4 = [8, 10, 18, 19, 20, 22, 23, 24]$.

2.3. Dynamic modeling

We now consider a model of a brain region constituted of N identical interconnected subregions of neurons each of which is represented by a Rossler nonlinear oscillator as proposed in Mazel et al [29]. So for EEG data of series 400s–440s, we can establish the following system of ordinary differential equations for seizure phase:

$$\dot{x}_i(t) = -\omega y_i(t) - z_i(t) + \sum_{j \in A_k, j \neq i} [\varepsilon_{ji}(h)(x_j(t) - x_i(t))] + x_d(t - \tau_k), \quad i \in A_k, \quad (2)$$

$$\dot{y}_i(t) = \omega x_i(t) + \alpha y_i(t), \quad (3)$$

$$\dot{z}_i(t) = b + z_i(t) \cdot [x_i(t) - \gamma], \quad (4)$$

$$\dot{h} = (1-h) \cdot [a_1(h-h_{eq})(h-h_{th}) + b_1 u_{exc}], \quad (5)$$

$$\dot{h}_{eq} = -a_2 h_{eq} + b_2 (h - h_{eq}), \quad (6)$$

where $x_i(t)$ represents the contribution of channel i ($i=1, \dots, M$) to the EEG recording, leading to

$$V_{EEG} = \sum_{i=1}^M \rho_i \cdot x_i \quad (7)$$

is the average model EEG for M channels. A_k is the cluster or subregion of 31 channels for 40s, while $k = 1, \dots, N$. In this case $M = 31$, $N = 4$ as mentioned above. Variable $y_i(t)$ and $z_i(t)$ represent internal states of the oscillator that are necessary to produce the oscillations with a suitable degree of freedom. The coefficient ρ_i is the relative contribution of channel i to the recording sensor. The scalar h denotes the synaptic strength in the region of interest in which h_{eq} represents a dynamic steady state, and h_{th} is the synaptic threshold. The product term $\varepsilon_{ji}(h)[x_j(t) - x_i(t)]$ represents the coupling effect of channel j on channel i , and the coupling factor ε_{ji} is described by:

$$\varepsilon_{ji} = \varepsilon_{ji}^{min} + \varepsilon_{ji}^0 \cdot h, \quad (8)$$

where ε_{ji}^{min} and ε_{ji}^0 are some constant values. Under normal conditions, desynchronization is assumed to be enhanced through the terms:

$$x_d(t - \tau_k) = A_d \sin\left(\frac{2\pi(t - \tau_k)}{T_d}\right); \quad \tau_k = \frac{2k\pi}{N}. \quad (9)$$

The signal x_d may be generated by a dedicated set of desynchronization neurons. The use of such a signal in synchronization or desynchronization control has been experimentally tested [38] and theoretically suggested [39, 40]. This desynchronization mechanism competes with the synchronization that is naturally induced by the connections. The outcome of this competition is highly dependent on the dynamics of the synaptic strength. Other constant parameters of our model are shown in Table 1.

2.4. Synaptic plasticity

Synaptic plasticity mechanisms involve both molecular and structural modifications that affect synaptic functions, either enhancing or depressing neuronal transmission. In Equation (4),(5), h denotes synaptic plasticity, h_{eq} is the steady state attractors and h_{th} is the synaptic threshold. Figure 4(a)–4(f) give the synaptic plasticity under different strength u_{exc} and duration of excitation signals T . After comparison the evolution of synaptic strength, these two values are fixed as $u_{exc} = 8$, $T = 90$ as the optimal values since $h_{th} = 0.5$ is an unstable equilibrium and is crucial in the definition of the transition and the establishment of the short-term plasticity. In this case synaptic plasticity can be reached in accordance with experimental observations. Later in the last section, we will test the model under different situations of synaptic plasticity.

2.5. Synchronization measurement

Neuronal activity at seizure presents a transient behavior of excessive or hypersynchronized neuronal pattern in all brain. The beginning of a seizure is expressed by excessive synchronized discharges of neurons within a cluster, and as time evolves, the adjacent and even remote clusters get involved. The dynamics of inherited seizures can be well characterized by synchronization measurement of EEG signals.

To measure the degree of synchronization in seizure activities, we use equal-time correlation matrix which is computed over moving time windows to analyze non-stationary measurement channels. Specifically, suppose $X_i(t_n)$ is the time series of i th channels, $t_n = n\tau$ is the detection time, then matrix C of a time window whose center time is t_c , is defined as follows:

$$C_{ij}(t_c) = \frac{1}{N_m} \sum_{n \in T(t_c)} [\tilde{X}_i(t_n) \tilde{X}_j(t_n)], \quad (10)$$

$$\tilde{X}_i(t_n) = \frac{X_i(t_n) - \bar{X}_i(t_n)}{\sigma_i}, \quad (11)$$

where $T(t_c)$ is the set of instant indices that belong to the time window centered at t_c , while N_m is the number of such time points. \bar{X}_i and σ_i denote the mean value and the standard deviation of the measurements captured in the time window of channel i separately.

Assuming the eigenvalues of matrix C are in ascending order $\lambda_1 \ \lambda_2 \ \dots \ \lambda_M$, then a synchronization indicator can be calculated by:

$$S = \frac{M}{M-1} \left[\frac{\lambda_M}{\sum_{i=1}^M \lambda_i} - \frac{1}{M} \right] \quad (12)$$

Particularly, if $S = 1$, then all channels are perfectly synchronized, while $S = 0$ denotes that all M channels are completely de-synchronized. Meanwhile, to verify the matching degree of model EEG and clinical EEG, we use another deformation of the variance σ to study. We calculate the model EEG and that of the channel FP1 of clinical EEG data for comparison since these 31 channels are in high synchronization during seizure. Number all the above $\sigma(t)$ in Eq. (11) captured in each time window in sequence and its maximum $\sigma(t)$, then

$$\langle \sigma \rangle = \frac{\sigma}{\max \sigma(t)} \quad (13)$$

for EEG of channel 1 and for model EEG to compare.

3. Numerical simulation

Regardless of seizure period and non-seizure period, the EEG signals of neonatal seizures show a train of burst and suppression waves. A valid model should satisfy these characters that the high amplitude spike and slow wave of irregular mixed outbreak always alternate with nearly flat suppression phase with statistics matching with clinical data. In the following, we give two simulation cases to test the validity of our modeling strategy.

3.1. 400s–440s

Firstly, Figure 5(b) is the model data V_{EEG} between 400s and 440s, showing the model EEG behaves similar to the clinical EEG which is shown in Figure 5(a) with rescaling. When seizures begin, V_{EEG} behaves oscillatory with high frequency and high amplitude. Then it follows by a quiescent period where neural activities become comparatively weakened. The ratio of resting time and seizure duration is a qualitative property of the model, which can reproduce that of clinical data during the resting and onset of seizure. Furthermore, Figure 5(c),(d) compare the parameter $\langle \sigma \rangle$ of both clinical EEG data from channel FP1 and model data which match well with each other. Considering the effect of noise in EEG environment, the spectrum of the model EEG with $SNR = 0.5$ (typical in EEG data) and real EEG are plotted as Figure 5(e),(f). We suppose the model window time is also 40s to compute the spectrum. They both display a dominate frequency around 3Hz, which is consistent with the main ISI (interspike interval) of EEG data is 0.4s.

3.2. 760s–800s

In the interest of validating of model, we continue to pre-process the EEG data of 760s–800s shown in Figure 1(b) which reflects a later stage of seizure onset. After the same data processing, the structure of connected graphs for EEG data in 760s–800s is obtained as shown in Figure 6. The matrix A_k of Equation (1) can be read as: ① $A_1 = [1, 2, 3, 4, 11, 12, 17, 26]$; ② $A_2 = [5, 7, 18, 19, 21, 23, 24, 31]$; ③ $A_3 = [6, 8, 9, 10, 13, 14, 15, 16, 20, 22, 27, 28, 29, 30]$; ④ $A_4 = [25]$. Notice that Figure 7 presents the comparison of channel group for case 400s–440s and case 760s–800s. As time goes on, the group assignment of connection strength may undergo changes but adjacent channels are more easily grouped in one cluster.

Then in our simulation, V_{EEG} and synchronous index S can be also calculated by our proposed model as shown in Figure 8(a),(b). We can see the synchronous index approximates to 1 during epileptic peaks, that is to say that 31 channels nearly reach complete synchrony. During interictal period synchronous index of 31 channels dropped suddenly, and the lowest is close to 0.1 which illustrates a high desynchrony. Hence we may conclude that the model captures essential physiological features of original data of epileptic seizures, reflecting the feasibility of our proposed model.

4. Network connection

Next, to test the relevance of the synaptic connection in our seizure model, we test two extreme connection situations for brain regions to understand the range and limitations of our model.

4.1. Fully connected structure

In one extreme case, we consider that every two channels are strongly connected (the number of connection group $N=1$). So the connection matrix is called all-one and the simulation results are shown in Figure 9(a),(b). We observe in this case there are some intrinsic differences between the real epilepsy data and simulation data. The seizure duration is too long and the interest time is too short, resulting in inconsistency with the clinical brain activities of epilepsy patients.

4.2. Fully disconnected structure

In another extreme case, we suppose 31 channels are completely uncorrelated (the number of connection group $N=31$). The connection matrix of brain regions is a null matrix. The numerical results of this case are shown in Figure 9(c),(d). Although the time duration of seizure and rest states is about the same as that of clinical seizure EEG, but the brain activities of interest is very different from the real features of epilepsy patients. The intensity is too high or too low to match the clinical observation on patients with epilepsy. During resting period, the amplitudes of our model EEG fluctuate too wide or too narrow to agree with the clinical EEG signals of typical seizure patients.

Taking the above two results of connectivity structure, we may understand the significance of the connection between different brain regions.

5. Synaptic plasticity

There is plenty of experimental evidences demonstrating that synaptic plasticity plays an essential role in epileptic seizures. From the modeling of synaptic plasticity, we know both h_{th} and U_{exc} are two key elements. Hence in this section, these parameters relevant to synaptic plasticity are analyzed in the epilepsy network from simulated data, using the EEG model of 400–440s as an example.

5.1. Synaptic threshold

It was reported that above a threshold a short-term plasticity state was reached [41], thus the synaptic threshold h_{th} can affect synaptic plasticity directly. We observed a variety of neuron

patterns by changing the synaptic threshold. With increasing synaptic threshold, the seizure period will also increase correspondingly seen as Figure 10. In a time window of 2000 simulation steps, we observe a transition from three short seizures to a continuous seizure state. Therefore, synaptic plasticity can strongly regulate the time duration of seizure activity. These results provide a positive clue of seizure therapy through hormone to modify synapses.

5.2. Excitatory signal

In Figure 5, the excitation signals U_{exc} is shown to affect synaptic plasticity. High frequency excitations lead to an increase in the mean synaptic efficiency. From Figure 11 we observe that, when the excitatory signal intensity is very small ($U_{exc} = 2$), synchronous oscillation occurred consistently. When the excitatory signal increases to $U_{exc} = 4$, only a short interest can be captured in the 2000 simulation steps following by a long seizure time. When the strength increases to $U_{exc} = 6$, brain electrical activity in patients with epilepsy tended to be in a normal activity level. Therefore, low frequency excitatory signal strength can make the synchronous activities excessively, causing over-synchronized discharges.

6. Conclusion

In this study we characterize the dynamic evolution of EEG activity during seizures through a modeling study. Our research enriches a simple dynamical model describing the epileptic seizure initiation through transition from interictal to ictal state in a brain predisposed to epilepsy. By analyzing the correlation connection of neuronal circuits during seizure of multi-channels, the subregions of brains in seizure patients are classified. As a result, our dynamical model adequately reproduces the brain electrical activities in patients with epilepsy, providing an understanding of the epilepsy characteristics from the dynamical view. To test how the model depends on connectivity structure we provide the situations of both fully-connected and fully non-connected channels. Finally, simulation results show that synaptic threshold and the excitatory signals both affect seizure time. For seizure prediction, a combination between reducing synaptic strength and enhancing desynchronization can probably be expected to achieve better seizure prevention for the short term.

Acknowledgments

This research was supported by the Start-up Scientific Research Foundation of Northwestern Polytechnical University: No. G2016KY0301 and the National Natural Science Foundation of China: No.11602192.

Research reported in this publication was also supported in part by the National Center for Advancing Translational Sciences of the National Institutes of Health under award number UL1TR001105. The content is solely the responsibility of the authors and does not necessarily represent the official views of the NIH. None of the acknowledged persons or institutions participated in the design and conduct of the study; collection, management, analysis, and interpretation of the data; or preparation, review, or approval of the manuscript; or decision to submit the manuscript for publication.

References

1. Schindler K, Wiest R, Kollar M, Donati F. EEG analysis with simulated neuronal cell models helps to detect pre-seizure changes. *Clinical Neurophysiology*. 2002; 113(4):604–614. [PubMed: 11956006]

2. Sitges M, Aldana BI, Gmez CD, Nekrassov V. The antidepressant sertraline prevents the behavioral and EEG changes induced in two animal models of seizures. *Epilepsy and Behavior*. 2012; 25(4): 511–516. [PubMed: 23153716]
3. Zandi AS, Tafreshi R, Javidan M, et al. Predicting epileptic seizures in scalp EEG based on a variational Bayesian Gaussian mixture model of zero-crossing intervals. *IEEE Transactions on Biomedical Engineering*. 2013; 60(5):1401–1413. [PubMed: 23292785]
4. Feeney DM, Walker AE. The prediction of posttraumatic epilepsy a mathematical approach. *Formerly Archives Neurology*. 1979; 36(1):8–12.
5. Yadav R, Swamy MNS, Agarwal R. Model-based seizure detection for intracranial EEG recordings. *IEEE Transactions on Biomedical Engineering*. 2012; 59(5):1419–1429. [PubMed: 22361656]
6. Yang A, Arndt DH, Berg RA. Development and validation of a seizure prediction model in critically ill children. *Seizure: European Journal of Epilepsy*. 2015; 25:104–116. [PubMed: 25458097]
7. Gadhomi K, Lina JM, Gotman J. Seizure prediction in patients with mesial temporal lobe epilepsy using EEG measures of state similarity. *Clinical Neurophysiology*. 2013; 124:1745–1754. [PubMed: 23643577]
8. Liu A, Hahn JS, Heldt GP, Coen RW. Detection of neonatal seizures through computerized EEG analysis. *Electroencephalography and Clinical Neurophysiology*. 1992; 82(1):30–37. [PubMed: 1370141]
9. Clancy RR, Legido A, Lewis D. *Epilepsia. Occult Neonatal Seizures*. 1988; 29(3):256–261.
10. Painter MJ, Scher MS, Stein AD, et al. Compared with phenytoin for the treatment of neonatal seizures. *The New England Journal of Medicine*. 1999; 341:485–489. [PubMed: 10441604]
11. Gergory L, Nicolas JL, Gairisa CL, et al. Consequences of neonatal seizures in the rat: Morphological and behavioral effects. *Annals of Neurology*. 1998; 44(6):845–857. [PubMed: 9851428]
12. Somogyvari Z, Barna B, Szasz A. Slow dynamics of epileptic seizure: Analysis and model. *Neurocomputing*. 2001; 38:921–926.
13. Ursino M, LaCara GE. Travelling waves and EEG patterns during epileptic seizure: Analysis with an integrate-and-fire neural network. *Journal of Theoretical Biology*. 2006; 242(1):171–187. [PubMed: 16620870]
14. Gardner AB, Kaelbling LP. One-Class novelty detection for seizure analysis from intracranial EEG. *Journal of Machine Learning Research*. 2006; 7(6):1025–1044.
15. James R, Williamson JR, Blissa DW, et al. Seizure prediction using EEG spatiotemporal correlation structure. *Epilepsy Behavior*. 2012; 25(2):230–238. [PubMed: 23041171]
16. Mormann F, Kreuz T, Rieke C, et al. On the predictability of epileptic seizures. *Clinical Neurophysiology*. 2005; 116:569–587. [PubMed: 15721071]
17. Mormann F, Andrzejak R, Elger C, et al. Seizure prediction: the long and winding road. *Brain*. 2007; 130:314–333. [PubMed: 17008335]
18. Celka P, Boashash B, Colditz P. processing and time-frequency analysis of newborn EEG seizures. *IEEE Engineering in medicine and Biology Magazine*. 2001; 20(5):30–39. [PubMed: 11668894]
19. Lehnertz K, Andrzejak RG, Arnhold J, et al. Nonlinear EEG analysis in epilepsy: Its possible use for interictal focus localization, seizure anticipation, and prevention. *Clinical Neurophysiology*. 2001; 18(3):209–222.
20. Samanwoy, GD. Thesis (PhD). The Ohio State University; 2007. Models of EEG data mining and classification in temporal lobe epilepsy: Wavelet-chaos-neural network methodology and spiking neural networks.
21. Hopkins A, Davies P, Dobson C. Mathematical models of patterns of seizures their use in the evaluation of drugs. *Formerly Archives Neurology*. 1985; 42(5):463–467.
22. Thomas EM, Temko A, Lightbody G, et al. Gaussian mixture models for classification of neonatal seizures using EEG. *Physiological Measurement*. 2010; 31(7):1047–1064. [PubMed: 20585148]
23. Gonzalez-Ramirez LR, Ahmed OJ, Cash SS, et al. A biologically constrained, mathematical model of cortical wave propagation preceding seizure termination. *Plos Computational Biology*. 2015; 11(2):e1004065. [PubMed: 25689136]

24. Taylor PN, Baier G. A spatially extended model for macroscopic spike-wave discharges. *Journal of Computational Neuroscience*. 2011; 31(3):679–684. [PubMed: 21556886]
25. Taylor, PN., Baier, G., Cash, S., et al. A model of stimulus induced epileptic spike-wave discharges. *Computational Intelligence, Cognitive Algorithms, Mind, and Brain, 2013 IEEE Symposium on IEEE*; 2013; p. 53-59.
26. Chen M, Guo DQ, Wang TB, et al. Bidirectional control of absence seizures by the basal ganglia: a computational evidence. *PLoS Computational Biology*. 2014; 10(3):e1003495. [PubMed: 24626189]
27. Leite JP, Neder L, Arisi GM, et al. Moreira Plasticity, synaptic strength, and epilepsy: what can we learn from ultrastructural data? *Epilepsia*. 2005; 46(5):134–141. [PubMed: 15987268]
28. McNamara JO. Cellular and molecular basis of epilepsy. *Journal of Neuroscience*. 1994; 14:3413–3425. [PubMed: 8207463]
29. Mazen A, James SW, Graham CG. Synaptic plasticity-based model for epileptic seizures. *Automatica*. 2011; 47(6):1183–1192.
30. Logothetis NK. What we can do and what we cannot do with fMRI. *Nature*. 2008; 453:869–878. [PubMed: 18548064]
31. He B, Lian J. High-resolution spatio-temporal functional neuroimaging of brain activity (Review). *Critical Review in Biomedical Engineering*. 2002; 30:283–306.
32. Nunez, PL. *Electric fields in the brain: the neurophysics of EEG*. New York, NY: Oxford University Press; 1981.
33. Grave de Peralta MR, Gonzalez Andino SL, Morand S, et al. Imaging the electrical activity of the brain: ELECTRA. *Human Brain Mapping*. 2000; 9:1–12. [PubMed: 10643725]
34. Shellhaas R, Clancy R. Characterization of neonatal seizures by conventional EEG and single-channel EEG. *Clinical Neurophysiology*. 2007; 118:2156–2161. [PubMed: 17765607]
35. Pascual JM, Ronen GM. Glucose Transporter Type I Deficiency (G1D) at 25 (1990–2015): Presumptions, Facts, and the Lives of Persons With This Rare Disease. *Pediatric neurology*. 2015; 53(5):379–393. [PubMed: 26341673]
36. Pascual JM. Genetic Gradients in Epileptic Brain Malformations. *JAMA Neurolog*. 2016 May 9. doi: 10.1001/jamaneurol.2016.1039
37. Schindler K, Leung H, Elger ChE, et al. Assessing seizure dynamic by analyzing the correlation structure of multichannel intracranial EEG. *Brain*. 2007; 130:65–77. [PubMed: 17082199]
38. Lian J, Shuai J, Durand DM. Control of phase synchronization of neuronal activity in the rat hippocampus. *Journal of Neural Engineering*. 2004; 1:46–54. [PubMed: 15876622]
39. Rosenblum MG, Pikovsky AS. Delayed feedback control of collective synchrony—an approach to suppression of pathological brain rhythms. *Physical Review E*. 2004; 70(4):041904.
40. Hauptmann C, Omelchenko O, Popovych OV, et al. Control of spatially patterned synchrony with multisite delayed feedback. *Physical Review E*. 76(6):066209.
41. Thomson AM. Activity-dependent properties of synaptic transmission at two classes of connections made by rat neocortical pyramidal. *Journal of Physiology*. 1997; 502:131–147. [PubMed: 9234202]

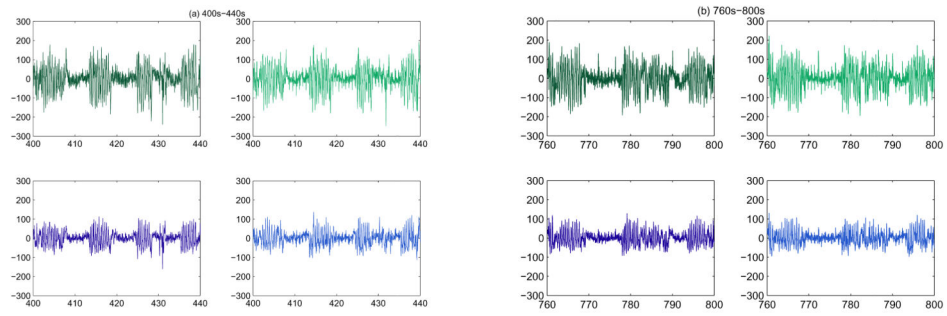
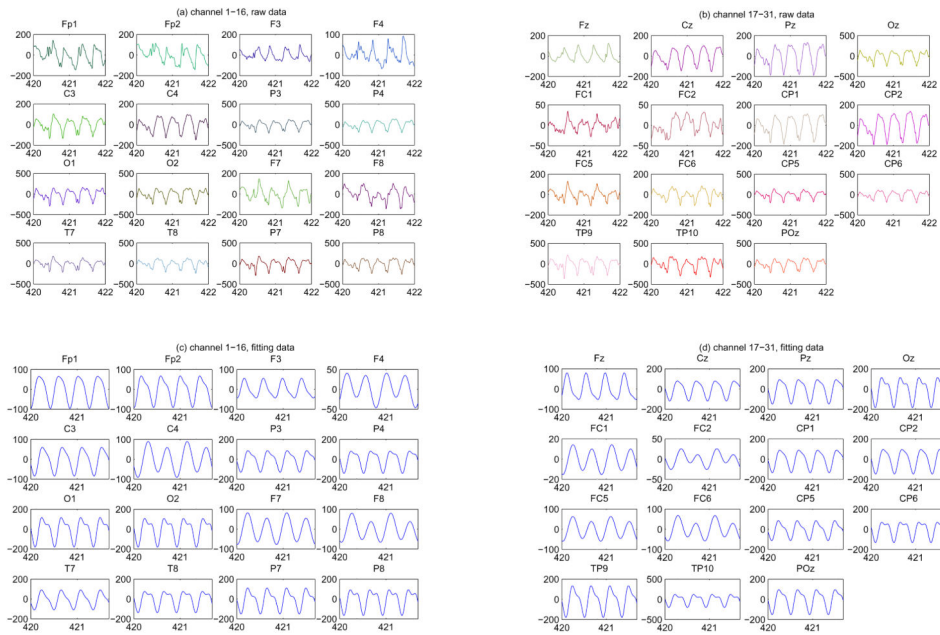


Figure 1. Sample EEG data during seizure periods. (a) 40s EEG data of the first four channels for 400s–440s, left above-Fp1, right above-Fp2, left below-F3, right below-F4. (b) 40s EEG data of the first four channels for 760s–800s, left above-Fp1, right above-Fp2, left below-F3, right below-F4.



5

Figure 2. Pre-processing of EEG data using de-noise and Fourier filter. (a) Collection of raw EEG data of channel 1–16 for 420s–422s. (b) Collection of raw EEG data of channel 17–31 for 420s–422s. (c) Fourier fitting data of channel 1–16 for 420s–422s. (d) Fourier fitting data of channel 17–31 for 420s–422s.

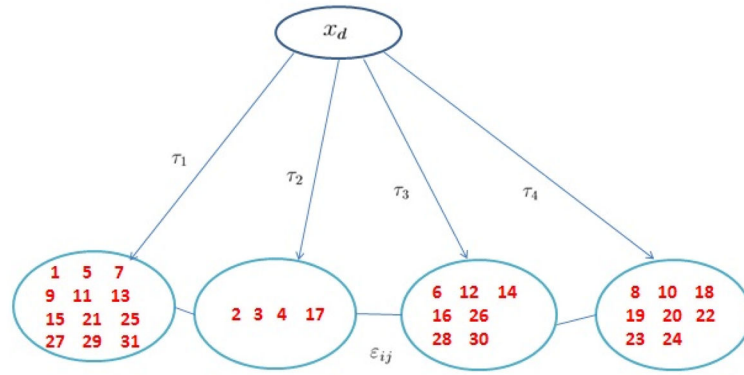


Figure 3.

Network structure of 31 channels for EEG data from 400s–440s. The feedforward based desynchronization mechanism relies on the different delays affecting the transmission of a desynchronization oscillator signal x_d .

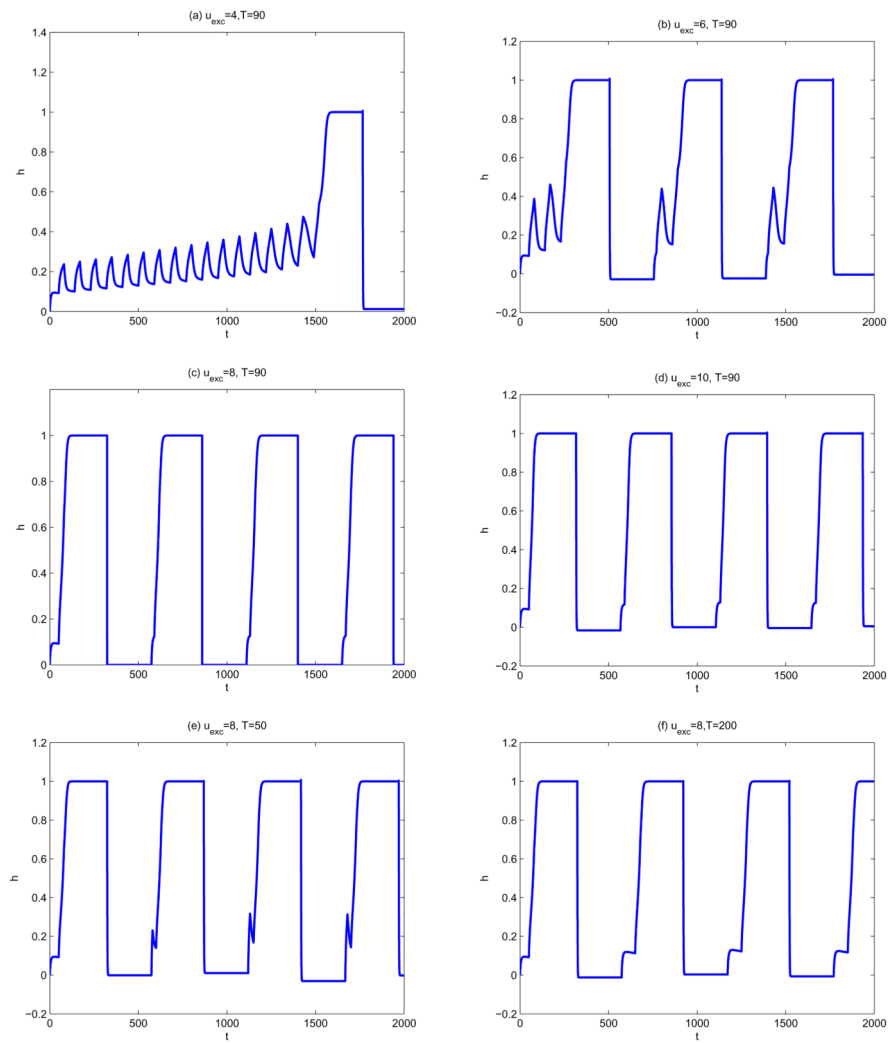


Figure 4. The time series of synaptic plasticity $h(t)$ under different conditions. The plasticity presents a periodic pattern after an initial period in several group of parameters. (a) $u_{exc} = 4$, $T = 90$. (b) $u_{exc} = 6$, $T = 90$. (c) $u_{exc} = 8$, $T = 90$. (d) $u_{exc} = 10$, $T = 90$. (e) $u_{exc} = 8$, $T = 50$. (f) $u_{exc} = 8$, $T = 200$.

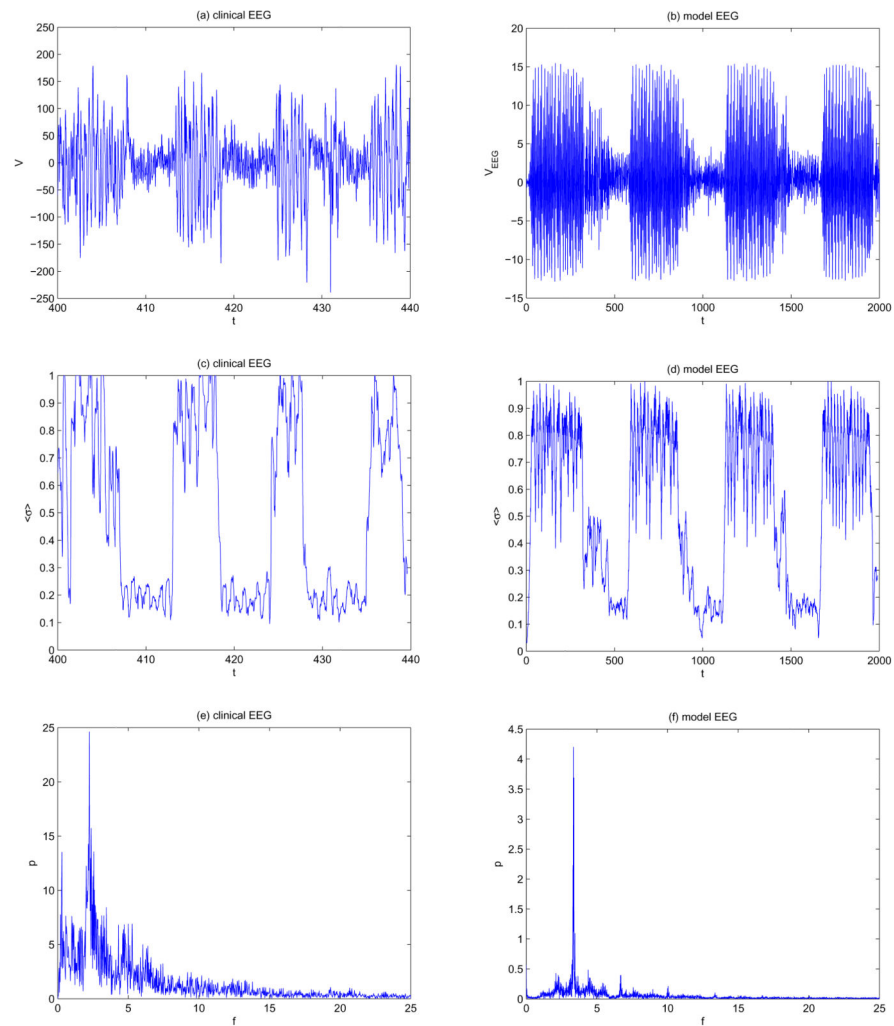


Figure 5. Comparison of clinical EEG data and model EEG data for time period 400–440s. (a) Clinical EEG data of channel Fp1 for period 400–440s. (b) Model data V_{EEG} of 400–440s with $h_{th} = 0.5$, $u_{exc} = 8$, $T = 90$. (c) Normalized variance $\langle \sigma \rangle$ of clinical EEG of channel Fp1 for period 400–440s. (d) Normalized variance $\langle \sigma \rangle$ of model EEG of 400–440s. (e) Spectrum of clinical EEG of the first channel for period 400–440s. (f) Spectrum of model EEG of 400–440s with $snr = 0.5$.

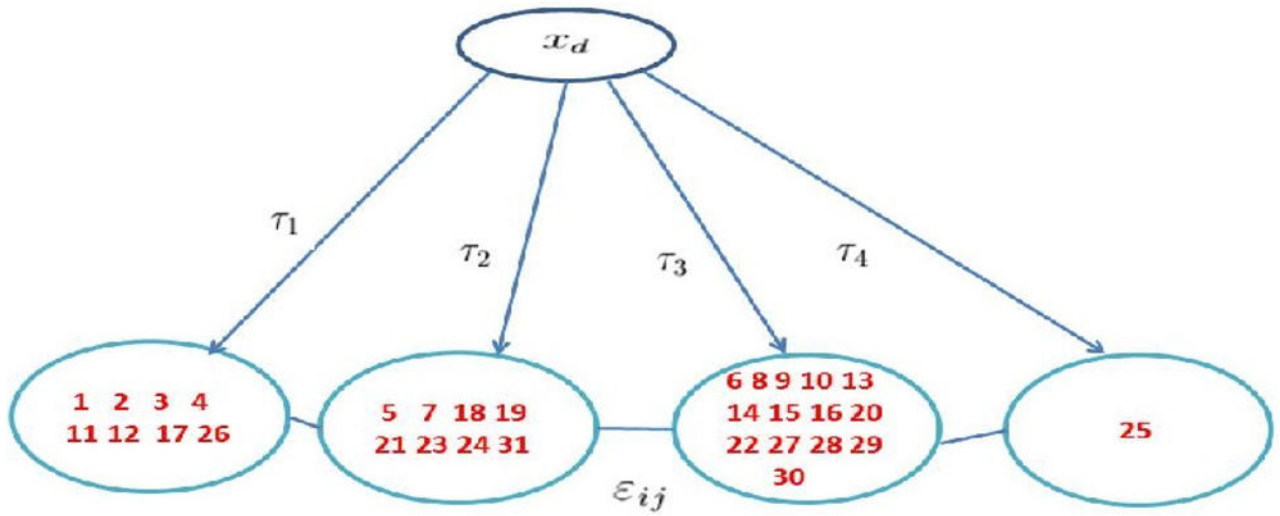


Figure 6. Network structure of 31 channels for 760s–800s.

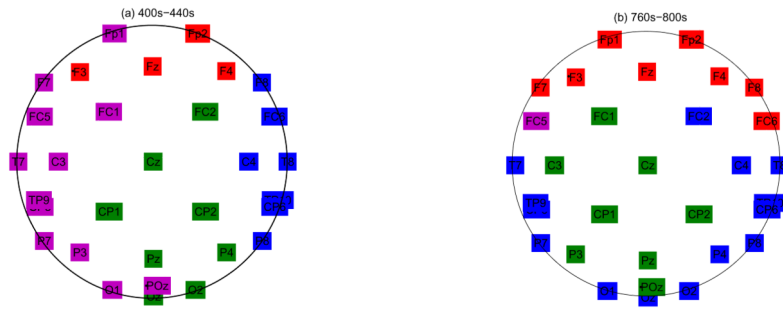


Figure 7. Relationship of different channels under the computation of correlation efficient. (a) case of 400s–440s. (b) case of 760s–800s. Channels in the same color in one subplot means they are in one connection group.

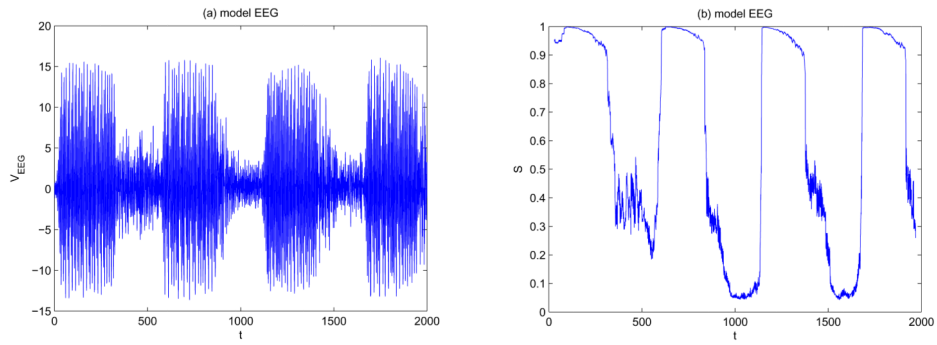


Figure 8. Model results under $h_{th} = 0.5$, $u_{exc} = 8$, $T = 90$, which match well with the clinical phenomenon of seizure. (a) Model EEG V_{EEG} of 760–800s. (b) Synchronous index S of model EEG.

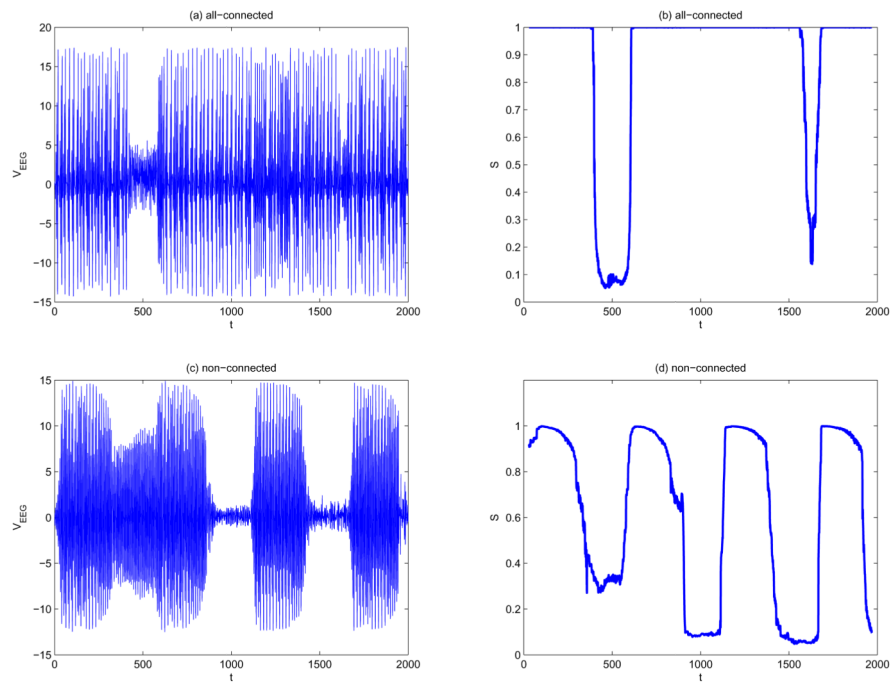


Figure 9.

Model results V_{EEG} and synchronous index S under two extreme connection structure. $u_{exc} = 4$, $T = 90$, $h_{th} = 0.5$. (a) V_{EEG} , $N=1$, all 31 channels are in one group. (b) S , $N=1$, all 31 channels are in one group. (c) V_{EEG} , $N=31$, 31 channels are independent and are divided into 31 groups. (d) S , $N=31$, 31 channels are independent and are divided into 31 groups.

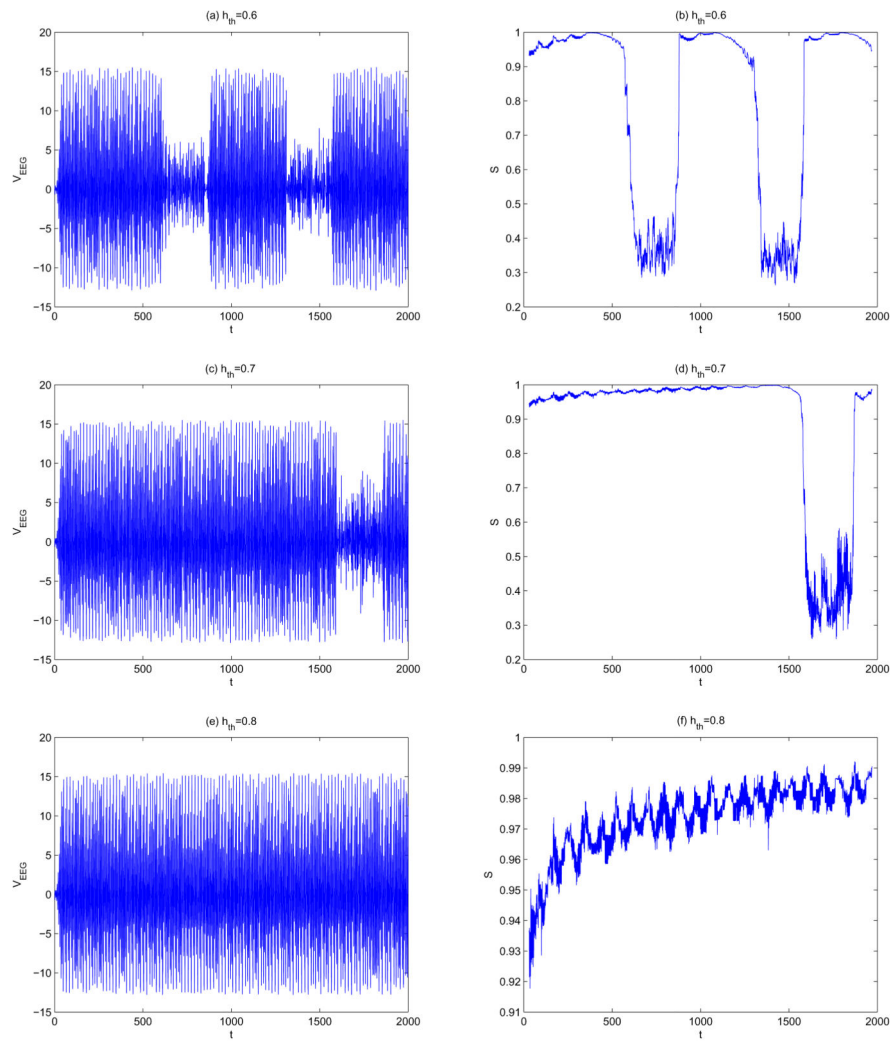


Figure 10.

Model $V_{EEG} = V_{EEG}(t)$ and synchronous index $S = S(t)$ under different synaptic plasticity threshold when $0 \leq t \leq 2000$, $u_{exc} = 4$, $T = 90$. (a) V_{EEG} , $h_{th} = 0.6$. (b) S , $h_{th} = 0.6$. (c) V_{EEG} , $h_{th} = 0.7$. (d) S , $h_{th} = 0.7$. (e) V_{EEG} , $h_{th} = 0.8$. (f) S , $h_{th} = 0.8$.

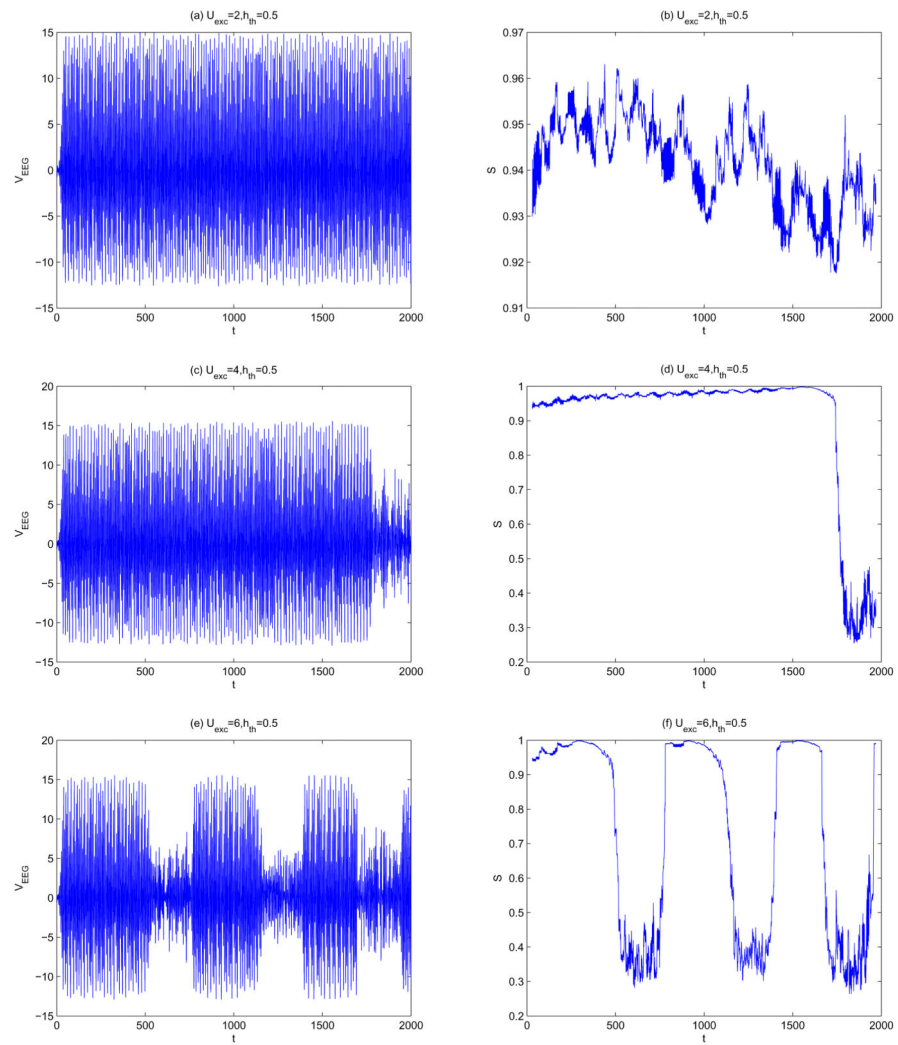


Figure 11.

V_{EEG} and synchronous index S under different excitation signals, $h_{th} = 0.5$. (a) V_{EEG} , $U_{exc} = 2$, $T = 90$. (b) S , $U_{exc} = 2$, $T = 90$. (c) V_{EEG} , $U_{exc} = 4$, $T = 90$. (d) S , $U_{exc} = 4$, $T = 90$. (e) V_{EEG} , $U_{exc} = 6$, $T = 90$. (f) S , $U_{exc} = 6$, $T = 90$.

Table 1

Model parameters

parameter	value	parameter	value	parameter	value
ω	1.00	b	0.20	A_d	1.00
α	0.15	e_{ij}	0.00	T_d	6.00
γ	8.50	$\varepsilon_{i,j}^0$	0.21	τ_i	$2i\pi/3$
a_1	0.50	b_1	0.005	a_2	0.0013
U_{exc}	8.00	T	90.0	h_{th}	0.50